SLIDING SCATTERING CENTER MODEL FOR EX-TENDED STREAMLINED TARGETS

Kun-Yi Guo[1, 2], Qi-Feng Li[1], Xin-Qing Sheng[1, *], and Marina Gashinova[2]

[1]Center for Electromagnetic Simulation, School of Information and Electronics, Beijing Institute of Technology, Beijing 100081, China

[2]Electronic, Electrical and Computer Engineering (EECE), University of Birmingham, Birmingham B15 2TT, UK

Abstract—The knowledge of amplitude and location of sliding scattering centers is necessary for low detectable streamlined targets in many applications, such as precise estimation of shape or velocity of targets, and also target tracking and recognition. Based on the thorough analysis of scattering characteristics, the scattering center features of streamlined targets are presented which demonstrate the dependence of location and amplitude on the target orientation relative to the radar. Then based on these features, an accurate scattering center model for streamlined targets is proposed. The parameters of this model is estimated by genetic algorithm, and then the given model with estimated parameters is validated by full wave numerical method allowing precise backscattered data computation.

1. INTRODUCTION

The signatures shown in range profiles, radar images and time-frequency presentations (TFR) are determined by the scattering characteristics of the observed scenario including targets and environments, though they are also affected by the resolutions, the level of side-lobes and noise induced by external interference to some extent. The scattering characteristics generally refer to the amplitude and phase distribution characteristics of scattered field in frequencies and orientations. Different models were proposed for describing the features of scattered waves by the complex electromagnetic environments [1–5]. For extended target in free space, scattering center

model [7–12] is the most effective model for describing the features of scattered waves by the target. For higher accuracy of radar signal simulation or parameter estimation, the scattering center model should be built based on the scattering characteristics of the extended target rather than the signatures shown in radar or optical images on the consideration of target as a set of fixed scattering centers.

From the view of radar signal processing, scattering center model is more practical than scattering characteristics as it is provides straight relationship between the signatures in radar images and the physical features of targets, and thus are broadly used in many radar applications, such as shape, velocity and other physical parameters estimation [6, 7], automatic target recognition (ATR) [8, 9], radar image interpretation [10–12], and radar data compression [13–15], etc.. The scattering centers due to scattering sources at discontinuities of surface, such as spires, corners and gaps, etc., have been of concern in applications of geometry parameter estimation, radar target tracking and recognition for decades [16–18], for their scattering characteristics being stable within a relatively wide radar observation angle. The existing scattering centers models include the classical GTD (Geometrical Theory of Diffraction) based model [19] and the attributed scattering center model [20, 21]. The latter additionally provides the intensity dependence of scattering center on orientation of target relative to radar.

Many modern radar targets are designed to have a streamlined shape for two reasons: to reduce the aerodynamic resistance and to lower target detectability. Scattering centers on streamlined surface have the tendency of sliding with the change of observation directions by radar, which is not considered in the existing scattering models. The sliding of scattering center leads to the changes of signatures in radar image and also the changes of Doppler frequencies, which results in serious problems in parameter estimation, target tracking and recognition [22].

To tackle this problem, the features of scattering centers on streamlined target are investigated based on a thorough analysis of scattering characteristics. For a better description of these features, an appropriate model of sliding scattering centers is presented in this paper. A parameter estimation approach based on this model is also demonstrated. Then in order to validate the presented model, the results of simulations based on this model are compared with the results based on the accurate backscattered data computed by the full wave numerical method, namely hybrid finite element-boundary integral-multilevel fast multipole algorithm (FE-BI-MLFMA) [23–25].

This paper is organized as follows. Section 2 presents the features

of the scattering center on the streamlined smooth surface through the analysis of scattering characteristics. Section 3 introduces the sliding scattering center model, which can accurately describe the amplitude and location of scattering centers on streamlined smooth surface. Then we verify the suggested model in Section 3 by a comparison of the results of simulations based on this model and the results based on FE-BI-MLFMA. Then the discussion of the obtained results is presented in Section 4.

2. FEATURES OF SCATTERING CENTERS OF STREAMLINED TARGETS

For target with streamlined smooth surface, the change patterns of sliding scattering centers in amplitude and location are determined essentially by its particular scattering characteristics. To establish the relationship between the scattering characteristics and features of scattering centers, the scattering characteristics of two targets with different smooth surfaces are investigated here. Their geometry structures are illustrated in Fig. 1. Target I has a shape of a half-ellipse. Target II has a shape of revolution body with the surface defined by the revolution of a curve relative to axis $\hat{z}$: $z = -83.3945y^4 + 74.5158y^3 - 24.7709y^2 + 0.6062y + 2.59$, $y \in [0, 0.55]$. The geometrical parameters are set as: $h_1 = 1.6\,\mathrm{m}$, $r_1 = 0.4\,\mathrm{m}$; $h_2 = 2.6\,\mathrm{m}$, $r_2 = 0.55\,\mathrm{m}$. The top of Target II is blunted in solid molding for better mesh and higher
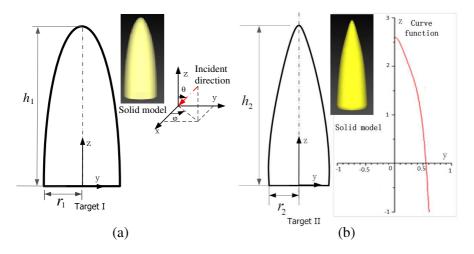

Figure 1. Geometry structures of the two targets. (a) Target I. (b) Target II.

accuracy in electromagnetic computation.

The backscattered field computed by FE-BI-MLFMA is denoted as $E^s(\theta, \phi, f)$. The orientation angle (θ, ϕ) is defined in Fig. 1. Both of the two targets are rotationally symmetrical, which means that the scattering fields for different ϕ are all the same, therefore $E^s(\theta, \phi, f)$ can be simplified to $E^s(\theta, f)$. The amplitude of backscattered field is indicated by radar cross section (RCS) and the phase of $E^s(\theta, f)$ is indicted by the phase angle within $[0, 360°]$, as presented in Figs. 2 and 3, where $\theta = 0° \sim 360°$; frequency bands for Targets I and II are $[2\,\text{GHz}, 4\,\text{GHz}]$ and $[1\,\text{GHz}, 2\,\text{GHz}]$ respectively. The scattering mechanisms by two targets are defined as optical scattering for the
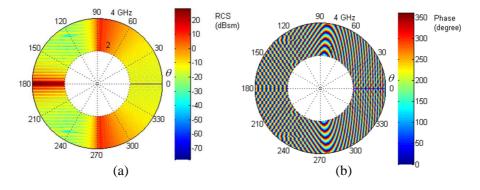

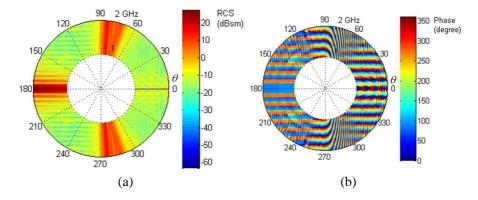Figure 2. The scattering characteristics of Target I. (a) RCS. (b) Phase angle.

Figure 3. The scattering characteristics of Target II. (a) RCS. (b) Phase angle.

given frequency band, so the analysis given in this paper is restricted by the optical scattering region consideration.

The scattering characteristics of θ within $[0, 90°]$ which are more concerned in practical application, hence are investigated particularly in the following. According to Fig. 2(a), it can be seen that the RCS of Target I increase gradually while θ increases from $0°$ to $90°$. To interpret this phenomenon, the amplitude of backscattered field and the reciprocal of curvature ($1/\kappa$, κ is the curvature) of the smooth surface are shown alongside in Fig. 4. The results show clear conformity of two curves. The increase of $1/\kappa$ accordingly corresponds to the increase of the back-reflection perpendicular to the curved surface (called perpendicular back-reflection for short), hence the result in Fig. 4 implies that main contributions into the backscattered field are made by the perpendicular back-reflection, in other words, the dominant scattering center of the curved surface is primarily caused by the perpendicular back-reflection. Fig. 3(a) and Fig. 5 demonstrate a bit different behavior of the RCS (or the amplitude of backscattered field) of Target II, slightly decreasing in the vicinity of $\theta = 0°$ and then increasing gradually while θ increases. The reason is that the top of the solid model is blunted, so the $1/\kappa$ of the top of the solid model is larger than the analytical value defined by the curve function.
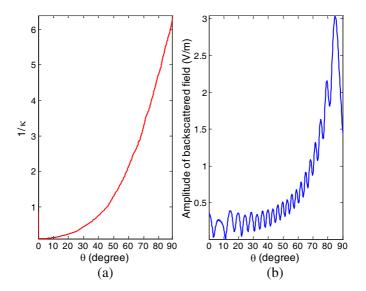

Figure 4. Target I: Comparison between amplitude of backscattered field and $1/\kappa$. (a) $1/\kappa$ defined by the surface function. (b) Amplitude of backscattered field.
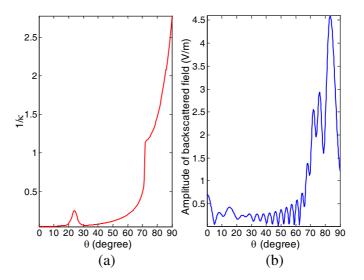
Figure 5. Target II: Comparison between amplitude of backscattered field and $1/\kappa$. (a) $1/\kappa$ defined by the surface function. (b) Amplitude of backscattered.

In fact, the results shown in Figs. 2–5 verify the broadly approved conclusion for optical scattering that the scattering can be approximately computed by ray tracing approach. We, however, will extend this concept analyzing how the location and amplitude of scattering center on smooth surface change when the incident direction of radar wave varies. The dominant scattering center of the curved surface is caused by perpendicular back-reflection, therefore, the location of scattering center on curved surface corresponds to the place where perpendicular back-reflection occurs, and slides when radar observation directions changes, as illustrated in Fig. 6, the sliding scattering center on the smooth surface is denoted as SC1; the amplitude of sliding scattering center is related to the size of the local surface contributing into the perpendicular back-reflection, therefore, is determined by both its particular curved surface function and radar observation directions. The dependent features of location and amplitude of scattering center on radar observation directions for streamlined target is not covered by exiting scattering center models.

If another scattering center, except for SC1, is presented nearby, for example when $\theta = 70° \sim 90°$ in Figs. 4 and 5, the change of the amplitude of backscattered field is not coherent with the change of $1/\kappa$, because the backscattered field is now composed by surface reflection and edge scattering.
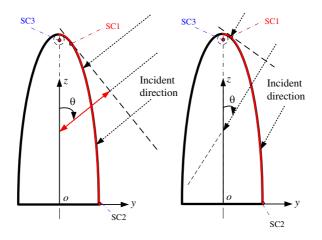
Figure 6. Illustration of the sliding of scattering center on the smooth surface.

In order to represent the characteristics of sliding scattering centers, the TFRs of backscattered waves while two targets rotating along $\hat{x}$ axis in plane of z-y are given in Figs. 7 and 8. The parameters are set as: the duration time is 1 s; the rotation frequency is 0.25 Hz; the initial position of rotational axis is $\hat{z}$; the operational frequencies are 4 GHz and 2 GHz for Target I and II respectively. The joint time-frequency method used in this paper is the short-time Fourier transform [26, 27].

To validate that the location of the scattering center corresponds to the place where perpendicular back-reflection occurs, the simulated Doppler frequency curve of sliding scattering center SC1 is compared with the real signatures in TFR of backscattered signal from the extended target, as shown in Figs. 7 and 8. The results show prefect agreement between them. To show the distinctive characteristics of the sliding scattering center from the fixed scattering center, the Doppler frequency curves of the fixed points (denoted as SC3 in Fig. 6) on the top of two targets are also shown in Figs. 7 and 8. The difference of Doppler frequencies between sliding and fixed scattering center implies that errors will be caused in velocity estimation based on Doppler frequency if the sliding scattering center is considered to be fixed on target.

As a conclusion we can state, that dominant scattering centers on target with streamlined surface are primarily caused by perpendicular back-reflection. The locations where dominant perpendicular back-reflections arise will change with orientations, therefore, the scattering
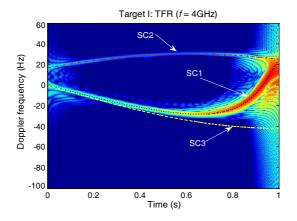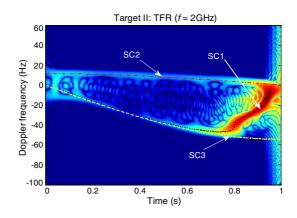
Figure 7. TFR of Target I.

Figure 8. TFR of Target II.

centers slide along the surface while radar observation direction varies. The amplitude of sliding scattering center is proportional to the size of local surface contributing into perpendicular back-reflection, but it will be interfered by other scattering sources nearby, which makes the change pattern of amplitude hard to predict analytically by only simple forms of functions, such as sinc function and exponential function.

3. THEORETICAL BACKGROUND OF SLIDING SCATTERING CENTER MODEL

Comparing with the classical GTD model, the attributed scattering center model further provides the dependent amplitude of scattering

center on target orientation relative to radar. The attributed scattering center model is described by Eq. (1). In contrast to [20], this model describes three-dimensional distributed scattering centers for extended targets, and, therefore, the locations of scattering centers are expressed by vectors rather than scalar as in [20].

$$E^s(\xi(\theta,\phi), f; \vartheta) = \sum_{i=1}^{q} A_i \left(\frac{jf}{f_c}\right)^{\alpha_i} \exp(-2\pi f \gamma_i \sin \xi(\cdot))$$
$$\sin c\left(\frac{2\pi f}{c} L_i \sin(\xi(\cdot))\right) \exp\left(-j\frac{4\pi f}{c}\vec{r}_i \cdot \hat{n}_{los}\right) \quad (1)$$

In Eq. (1), $\xi(\theta,\phi)$ indicates the orientation of target relative to radar; q is the number of scattering centers; $\vec{r}_i = (x_i, y_i, z_i)$ is the vector of i-th scattering center; $\hat{n}_{los} = (\cos\theta\cos\phi, \cos\theta\sin\phi, \sin\theta)$ is the observation direction by radar; A_i is the amplitude of i-th scattering center; f_c is the central frequency; α_i is the parameter indicating the dependence on frequency; L_i indicates the effective length of distributed i-th scattering center; γ_i is the coefficient of the dependence on orientation. The dependence of the scattered field on the parameters are presented by $\vartheta = \left\{A_i, \vec{r}_i, \alpha_i, \gamma_i, L_i\right\}$.

The term $\left(\frac{jf}{f_c}\right)^{\alpha_i}$ in Eq. (1) can be further expressed as:

$$\left(\frac{jf}{f_c}\right)^{\alpha_i} = e^{\left(j\frac{\pi}{2}\alpha_i\right)} \left(\frac{f}{f_c}\right)^{\alpha_i} \quad (2)$$

The exponential factor $e^{\left(j\frac{\pi}{2}\alpha\right)}$ is independent on frequency and orientation, therefore, will not affect the result of Fourier transform or joint time-frequency transform. Thus, it is ignored in the following analysis and the simplified version of Eq. (1) will be considered:

$$E^s(\xi, f; \vartheta) = \sum_{i=1}^{q} A_m^i(\xi; \vartheta) \left(\frac{f}{f_c}\right)^{\alpha_i} \exp\left(-j\frac{4\pi f}{c}(\vec{r}_i \cdot \hat{n}_{los})\right) \quad (3)$$

where

$$A_m^i(\xi; \vartheta) = A_i \exp\left(-2\pi f \gamma_i \sin(\xi)\right) \sin c\left(\frac{2\pi f}{c} L_i \sin(\xi)\right) \quad (4)$$

From Eqs. (1)–(4), it can be seen that the attributed scattering model has few limitations: first, in the phase related term, $\exp\left(-j\frac{4\pi f}{c}(\vec{r}_i \cdot \hat{n}_{los})\right)$, the location vector $\vec{r}_i = (x_i, y_i, z_i)$ is considered as being invariant to $\xi(\theta,\phi)$, which is not true for scattering centers on streamlined smooth surface; second, the amplitude $A_m(\xi; \vartheta)$

is expressed by simple functions, which can hardly describe the variation in the amplitude of sliding scattering center, due to the change of surface curvature or the interference by the coupled scattering in presence of multiple scattering centers.

According to the previous section, the scattering centers on smooth surface have two features: first, the location of scattering center slides with the change of orientation, which means that the location vector $\vec{r}_i$ should be a function of $\xi(\theta, \phi)$; second, the amplitude of scattering center changes when the curvature of smooth surface varies, and it gets more complex if other scattering sources are presented nearby.

Thus, we suggest a sliding scattering model for the target of smooth surface, as given by Eq. (5).

$$E^s(\xi, f; \vartheta) = A_s(\xi, P, Q)\left(\frac{f}{f_c}\right)^\alpha \exp\left(-j\frac{4\pi f}{c}\left(\vec{r}_i(\xi) \cdot \hat{n}_{los}(\xi)\right)\right) \quad (5)$$

In Eq. (5), the location vector $\vec{r}_i$ is now a function of ξ , and it can be derived based on the surface function of target, as given in appendix A; the amplitude $A_s(\xi, P, Q)$ is now described by a fractional polynomial function, as given by Eq. (6).

$$A_s(\xi, P, Q) = \frac{P_0 + P_1\xi + P_2\xi^2 + \ldots + P_n\xi^n}{Q_0 + Q_1\xi + Q_2\xi^2 + \ldots Q_{m-1}\xi^{m-1} + \xi^m} \quad (6)$$

where $P = [P_0, P_1, \ldots, P_n]$ and $Q = [Q_0, Q_1, \ldots, Q_{m-1}]$ are polynomial coefficient vectors. Based on the principle of model-based parameter estimation (MBPE) [28, 29], a fractional polynomial function has the ability of fitting any rational function, subject to polynomial order and coefficients. Therefore, the amplitude of sliding scattering center of any specific shape of streamlined target or the amplitude in presence of multiple scattering can be described in such a way. The scattering model given above is also suitable for the other kind of scattering center when the location of scattering centers is known *a priori*.

Higher polynomial orders in Eq. (6) are able to fit more complex function, but result in longer computation time and more possibility of local optimum in coefficients estimation. Therefore, to balance these factors, the polynomial orders are set as $n = 21$, $m = 20$ in this paper.

When target is rotationally symmetrical, scattering characteristics are independent on ϕ, so the orientation can be simplified to $\xi(\theta, \phi) = \theta$. We will mainly focus on the variation of scattering centers due to orientation and the frequency of the backscattered signal will be assumed not changing, so $(f/f_c)^\alpha = 1$. Actually, the variation of RCS is relatively small for streamlined targets (as shown in Figs. 2 and 3), so the results obtained in this paper can be expanded to a wider frequency band to some extent.

4. PARAMETER ESTIMATION OF THE SLIDING SCATTERING CENTER MODEL

In order to validate the suggested sliding scattering center model, the estimation of model parameters is implemented, and then the comparison of simulated results based on this model with the backscattered data computed by FE-BI-MLFMA is made. Both Targets I and II have two dominate scattering centers (marked as SC1 and SC2 in Fig. 6). SC1 is responsible for the perpendicular back-reflection on the surface and SC2 for back scattering by the bottom edge. Both of them are sliding scattering centers, however there is a difference as SC1 slides only if θ changes, while SC2 slides only if ϕ changes. Though the backscattering of SC1 and SC2 are interfered with each other when ordination angle θ approaching to $90°$, the backscattering intensity of SC1 can still be described by the fractional polynomial function given above. And since the estimation process of two scattering centers are generally the same, so parameters estimation of SC2 is ignored here.

Both nonparametric and parametric methods are usually used to estimate parameters of scattering centers. Nonparametric methods extract parameters of scattering centers directly from radar image without need to build scattering center model. So the accuracy of nonparametric methods is limited by the resolutions, ambiguity or errors of radar image. Parametric methods need first to build scattering center model and then estimate parameters of the model using optimization algorithms. Thus the accuracy of parametric methods is limited by the accuracy of the model used and the efficiency of the optimization algorithm itself. We used parametric methods, namely Genetic Algorithm [30–32], to estimate parameters P, Q (Eq. (6)) in the sliding scattering center model. To ensure the accuracy of estimation, six objective functions (OF) are employed in GA, as given below:

OF1: $y = \text{MSE}(\text{TFR}_o - \text{TFR}_e)$, where MSE means the Mean squared error; TFR_o and TFR_e indicate TFRs of the backscattered waves computed by FE-BI-MLFMA and the one simulated by described scattering center model respectively.

OF2: $y = -R(1,2) + 1$, where R is the matrix of correlation coefficient $R = corrcoef(\text{TFR}_o, \text{TFR}_e)$.

OF3: $y = \text{MSE}(\text{TFR}_o(\theta, f_D(\theta)) - \text{TFR}_e(\theta, f_D(\theta)))$, where $\text{TFR}_o(\theta, f_D(\theta))$ indicates the element of the matrix TFR_o at (row, column) $= (\theta, f_D(\theta))$; $f_D(\theta)$ indicates the Doppler frequency.

OF4: $y = -R(1,2) + 1$; where $R = corrcoef(\text{TFR}_o(\theta, f_D(\theta)), \text{TFR}(\theta, f_D(\theta)))$.

OF5: $y = \text{MSE}(\text{TFR}_o^d - \text{TFR}_e^d)$, where $\text{TFR}_{o,e}^d$ indicate the results after reducing the background noise. The calculation of $\text{TFR}_{o,e}^d$ is given in Appendix B.

OF6: $y = -R(1,2) + 1$; where $R = corrcoef(\text{TFR}_o^d, \text{TFR}_e^d)$.

The optimal solution is achieved when y tends to zero, in other words, MSE tends to zero and $R(1,2)$ approaches to 1, and they are required for both the comparison of $(\text{TFR}_o, \text{TFR}_e)$ and $(\text{TFR}_o(\theta, f_D(\theta)), \text{TFR}(\theta, f_D(\theta)))$.

The sliding center model with estimated parameters are used to simulate the backscattered signal of the targets, and then the TFR signatures of the simulated backscattered signal are compared with the TFR signatures of the accurate backscattered field computed by

Table 1. Results of cases under different objective functions for Target-I.

Target-I	$\text{TFR}_o, \text{TFR}_e$		$\text{TFR}_o(f_D), \text{TFR}_e(f_D)$	
cases	MSE	Correlation coefficient	MSE	Correlation coefficient
OF1	0.0478	0.9685	0.0478	0.9855
OF2	0.2225	0.8869	0.2225	0.9492
OF3	0.0516	0.9677	0.0516	0.9845
OF4	0.9685	0.8226	0.9685	0.8909
OF5	0.2703	0.8535	0.2703	0.9341
OF6	0.0544	0.9675	0.0544	0.9850

Table 2. Results of cases under different objective functions for Target-II.

Target-II	$\text{TFR}_o, \text{TFR}_e$		$\text{TFR}_o(f_D), \text{TFR}_e(f_D)$	
cases	MSE	Correlation coefficient	MSE	Correlation coefficient
OF1	0.1939	0.9057	0.0011	0.8972
OF2	0.2641	0.9130	0.0033	0.8777
OF3	0.1955	0.9052	6.4367e-4	0.9338
OF4	2.8552	0.7417	0.0249	0.9794
OF5	0.2251	0.9072	7.1972e-4	0.9309
OF6	0.2066	0.8988	0.0017	0.8642

FE-BI-MLFMA, as listed in Tables 1 and 2. The amplitudes of sliding scattering centers based on the estimated coefficients are presented in Figs. 9 and 10.

For Target I it can be seen from the Table 1 that all the results of six OFs have demonstrated good matching. The relative errors in amplitude among six results are less than 2 dB, and the relative errors among results of OF1, OF3 and OF6 are less than 0.5 dB. Target II has more complex surface function than Target I, and it can be seen from the Table 2 that only result of OF4 has relative large difference between TFR_o and TFR_e. The relative errors between OF1, OF3 and OF5 are less than 1 dB.

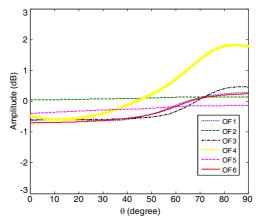The TFRs simulated by the suggested model with parameters

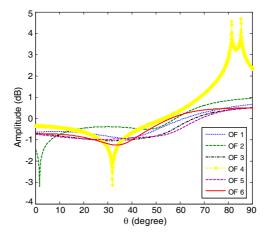**Figure 9.** The SC1 amplitude results of different OFs (Target I).

Figure 10. The SC1 amplitude results of different OFs (Target II).
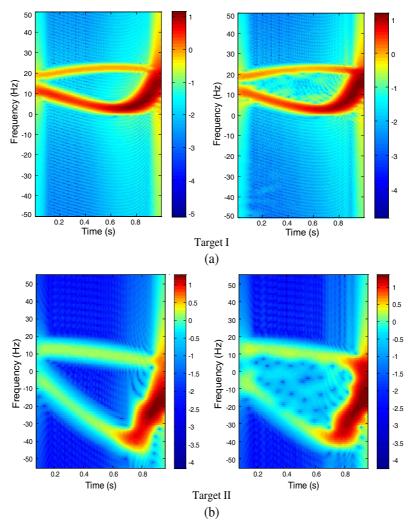
Target I

(a)

Target II

(b)

Figure 11. TFRs simulated (a) by suggested model and (b) by FE-BI-MLFMA.

estimated by OF5 are compared with that based on FE-BI-MLFMA computation in Fig. 11, which clearly demonstrates excellent agreement between these two approaches.

5. CONCLUSIONS

Scattering center features analysis of targets with streamlined surface has been undertaken in this paper. It has been shown that the

location of dominant scattering center on the curved surface which is largely responsible for the perpendicularly back-reflection by the curved surface slides with change of radar observation directions. The amplitude of sliding scattering center is related to the size of local surface contributing into the perpendicularly back reflecting; however it will be affected by the presence of other scattering sources situated nearby owing to the interaction between scattering sources.

Based on the above conclusions, the corrected scattering model for target of smooth surface has been suggested. In this model, the location of scattering center is presented as a function of orientation and can be derived from the function expressing the surface of target; the amplitude of such a scattering center is approximated by a fractional polynomial function which has the ability of fitting any rational function, subject to polynomial orders and coefficients.

To validate the suggested scattering model, the estimation of parameters of the model has been implemented, and the TFR signatures of the simulated signal by this model have been compared with that of accurate backscattered signal computed by FE-BI-MLFMA, demonstrating excellent agreement.

APPENDIX A.

Solve the group of functions (A1) for each given ξ, we can obtain location vector (A2).

$$
\begin{cases}
F(x, y, z) = 0 \\
\hat{n}(x, y, z) \times \hat{n}_{los}(\xi) = 0
\end{cases}
\tag{A1}
$$

where $F(x, y, z)$ is the surface function of the target.

The location of scattering centers:

$$
\vec{r}_i(\xi) = (x_s, y_s, z_s)
\tag{A2}
$$

where (x_s, y_s, z_s) is the solution of (A1).

APPENDIX B.

$$
\mathrm{TFR}_{o,e}^d =
\begin{cases}
\mathrm{TFR}_{o,e}, & \text{if } \mathrm{TFR}_{o,e} \geq N \\
0, & \text{if } \mathrm{TFR}_{o,e} < N
\end{cases}
\tag{B1}
$$

where N is the background noise of TFR_o:

$$
N = \max[hist(\mathrm{TFR}_o)]
\tag{B2}
$$

Here $hist$ indicates the intensity histogram of TFR_o [33].

ACKNOWLEDGMENT

REFERENCES

1. Liu, D. H., G. Kang, L. Li, Y. Chen, S. Vasudevan, W. Joines, Q. H. Liu, J. Krolin, and L. Carin, "Electromagnetic time-reversal imaging of a target in a cluttered environment," *IEEE Transactions on Antennas and Propagation*, Vol. 53, 3058–3066, 2005.

2. Fouda, A. E. and F. L. Teixeira, "Imaging and tracking of targets in clutter using differential time-reversal techniques," *Waves in Random and Complex Media,* Vol. 22, No. 1, 66–108, 2012.

3. Yavuz, M. E. and F. L. Teixeira, "Space-frequency ultrawideband time-reversal imaging," *IEEE Transactions on Geoscience and Remote Sensing*, Vol. 46, No. 4, 1115–1124, 2008.

4. Moustafa, K. and K. F. A. Hussein, "Performance evaluation of separated aperture sensor GPR system for land mine detection," *Progress In Electromagnetics Research*, Vol. 72, 21–37, 2007.

5. Bourgeois, J. M. and G. S. Smith, "A complete electromagnetic simulation of the separated-aperture sensor for detecting buried landmines," *IEEE Transactions on Antennas and Propagation*, Vol. 46, No. 10, 1419–1426, 1998.

6. Luo, Y., Q. Zhang, C. Qiu, X. Liang, and K. Li, "Micro-doppler effect analysis and feature extraction in ISAR imaging with stepped-frequency chirp signals," *IEEE Transactions on Geoscience and Remote Sensing*, Vol. 48, No. 4, 2087–2098, 2009.

7. Cheng, J., G. Gao, W. Ding, X. Ku, and J. Sun, "An improved scheme for parameter estimation of g° distribution model in high-resolution SAR images," *Progress In Electromagnetics Research*, Vol. 134, 23–46, 2013.

8. Zhou J. X., Z. G. Shi, X. Cheng, and Q. Fu, "Automatic target recognition of sar images based on global scattering center model," *IEEE Transactions on Geoscience and Remote Sensing*, Vol. 49, No. 10, 3713–3729, Oct. 2011.

9. Zhai, Y., J. Li, J. Gan, and Z. Ying, "A multi-scale local phase quantization plus biomimetic pattern recognition method for SAR automatic target recognition," *Progress In Electromagnetics Research*, Vol. 135, 105–122, 2013.

10. Feng, Z., L. Ying, Z. Qun, F. Y. Qian, and B. Y. Qing, "ISAR

imaging for avian species identification with frequency-stepped chirp signals," *IEEE Geoscience and Remote Sensing Letters*, Vol. 7, No. 1, 151–155. 2010.

11. Park, S.-H., J.-H. Lee, and K.-T. Kim, "Performance analysis of the scenario-based construction method for real target ISAR recognition," *Progress In Electromagnetics Research*, Vol. 128, 137–151, 2012.

12. Zhang, X., J. Qin, and G. Li, "SAR target classification using Bayesian compressive sensing with scattering centers features," *Progress In Electromagnetics Research*, Vol. 136, 385–407, 2013.

13. Chung, L. C., I. J. Gupta, W. D. Burnside, and C. T. Chang, "A data compression technique for scattered fields from complex targets," *IEEE Transactions on Antennas and Propagation*, Vol. 45, 1245–1251, Aug. 1997.

14. Carin, L., D. Liu, W. Lin, and B. Guo, "Compressive sensing for multi-static scattering analysis," *Journal of Applied Physics*, Vol. 228, No. 9, May 2009.

15. Potter, L. C., E. Ertin, J. T. Parker, and M. Certin, "Sparsity and compressed sensing in radar imaging," *Proceedings of the IEEE*, Vol. 98, No. 6, 1006–1020, 2010.

16. Potter, L. C., C. Da-Ming, R. Carriere, and M. J. Gerry, "A GTD-based parametric model for radar scattering," *IEEE Transactions on Antennas and Propagation*, Vol. 43, No. 10, 1058–1067, Oct. 1995.

17. Bhalla, R. and L. Hao, "Three-dimensional scattering center extraction using the shooting and bouncing ray technique," *IEEE Transactions on Antennas and Propagation*, Vol. 44, No. 11, 1445–1453, Nov. 1996.

18. Potter, L. C. and R. L. Moses, "Attributed scattering centers for SAR ATR," *IEEE Transactions on Image Processing*, Vol. 6, No. 1, 79–91, Jan. 1997.

19. Gerry, M. J., L. C. Potter, I. J. Gupta, and A. van der Merwe, "A parametric model for synthetic aperture radar measurements," *IEEE Transactions on Antennas and Propagation*, Vol. 47, No. 7, 1179–1188, Jul. 1999.

20. Chiang, H.-C., R. L. Moses, and L. C. Potter, "Model-based classification of radar images," *IEEE Transactions on Information Theory*, Vol. 46, No. 5, 1842–1854, Aug. 2000.

21. Zhou, J. X., H. Z. Zhao, Z. G. Shi, and Q. Fu, "Global scattering center model extraction of radar targets based on wideband measurements," *IEEE Transactions on Antennas and*

Propagation, Vol. 56, No. 7, 2051–2060, Jul. 2008.

22. Ma, L., J. Liu, T. Wang, Y. Z. Li, and X. S. Wang, "Micro-doppler characteristics of sliding scattering center on rotationally symmetric target," *Science China Information*, No. 41, No. 5, 606–616, 2011.

23. Sheng, X. Q., J. M. Jin, J. M. Song, C. C. Lu, and W. C. Chew, "On the formulation of the hybrid finite-element boundary-integral methods for 3D scattering," *IEEE Transactions on Antennas and Propagation*, Vol. 46, 303–311, 1998.

24. Sheng, X. Q., E. K.-N. Yung, C. H. Chan, J. M. Jin, and W. C. Chew, "Scattering from a large body with cracks and cavities by the fast and accurate finite-element boundary-integral method," *IEEE Transactions on Antennas and Propagation*, Vol. 48, 1153–1160, 2000.

25. Guo, K. Y. and X. Q. Sheng, "How to predict scattering and range profiles using complex targets with cavities," *IEEE Transactions on Aerospace and Electronic Systems*, Vol. 47, No. 1, 155–165, 2011.

26. Antonia, P. S., *Applications in Time-Frequency Signal Processing*, 1st Edition, 16–33, CRC Press, 2003.

27. *Time-Frequency Toolbox*, Jul. 2011, http://tftb.nongnu.org/.

28. Miller, E. K., "Model-based parameter estimation in electromagnetics-I: Background and theoretical development," *Appl. Comput. Electromagn. Soc. J.*, 40–63,1995.

29. Guo, K. Y. and X. Q. Sheng, "A precise recognition approach of ballistic missile warhead and decoy," *Journal of Electromagnetic Waves and Applications*, Vol. 23, Nos. 14–15, 1867–1875, 2009.

30. Larose, D. T., *Data Mining Methods and Models*, Wiley-IEEE Press, 2006.

31. Qing, L., E. J. Rothwell, Y.-F. Chen, and D. P. Nyquist, "Scattering center analysis of radar targets using fitting scheme and genetic algorithm," *IEEE Transactions on Antennas and Propagation*, Vol. 44, 198–207, Feb. 1996.

32. Hughes, E. J. and M. Leyland, "Using multiple genetic algorithms to generate radar point-scatterer models," *IEEE Transactions on Evolutionary Computation*, Vol. 4, No. 2, 147–163, Jul. 2000.

33. http://www.mathworks.co.uk/help/matlab/ref/hist.html, accessed Mar. 2013.